Hydrogen Generation from Weak Acids: Electrochemical and Computational Studies in the $[(\eta^5\text{-}C_5H_5)Fe(CO)_2]_2$ System

Greg A. N. Felton, Aaron K. Vannucci, Noriko Okumura, L. Tori Lockett, Dennis H. Evans,* Richard S. Glass,* and Dennis L. Lichtenberger*

Department of Chemistry, The University of Arizona, Tucson, Arizona 85721

Received April 26, 2008

$(\eta^5\text{-}C_5H_5)Fe(CO)_2H$ (FpH) is stable to weak acids such as acetic acid. However, reduction of FpH in acetonitrile in the presence of weak acids generates H_2 catalytically. Evidence for the catalytic generation of H_2 from just water also is observed. Since reduction of Fp_2 generates Fp^-, which can be protonated with weak acids, Fp_2 serves as a convenient procatalyst for the electrocatalytic production of H_2. Electrochemical simulations provide values for the key parameters of a catalytic mechanism for production of H_2 in this system. Protonation of Fp^- is found to be the rate-determining step preceding H_2 production. The wealth of structural, spectroscopic, and thermodynamic information available on the key Fp_2, Fp^-, and FpH species provide a variety of checkpoints for computational modeling of the catalytic mechanism. The computations give good agreement with the crystal structure of Fp_2, the IR spectra of Fp_2, Fp^-, and FpH, and the photoelectron spectra of Fp_2 and FpH. The computations also account well for the reduction potentials and equilibrium constants in the electrochemical simulations. The FpH^- anion is found to be susceptible to a direct and rapid attack by a proton to produce H_2 and the $Fp^\bullet$ radical, which is then reduced and protonated to continue the electrocatalytic cycle. This direct energetically downhill step of metal hydride protonation to produce molecular hydrogen may be common for sufficiently electron rich metal hydrides and/or sufficiently strong acids among many of the hydrogenase mimics reported thus far.

Introduction

Hydrogen can be produced from fossil fuels and biomass.[1] However, its formation from water photochemically,[2] biologically,[3] or electrochemically is imperative for realizing a renewable carbon-free energy economy. Such production of H_2 requires the discovery of new, efficient, and cheap catalysts. Much effort has been devoted to the development of active site analogues of the hydrogenases as well as the use of these enzymes themselves for H_2 generation.[4] The hydrogenases form three classes based on their active sites. The Hmd or [Fe] hydrogenases[5] bear one iron at their active site, do not contain iron−sulfur clusters, and catalyze the reversible reaction of N^5N^{10}-methylenyltetrahydromethanopterin with H_2 to N^5N^{10}-methylenetetrahydromethanopterin and H^+. The [NiFe] hydrogenases[6] contain one iron and one nickel in their active sites, while the [FeFe] hydrogenases[6] contain a dinuclear Fe−Fe center at their active sites. Both [NiFe] and [FeFe] hydrogenases catalyze the reversible reaction shown in eq 1,

$$2H^+ + 2e^- \rightleftharpoons H_2 \quad (1)$$

and both contain iron−sulfur clusters. Simpler catalysts based on [NiFe][7] and [FeFe][8] hydrogenases have been reported. Molybdenum sulfur dimers also serve as electrocatalysts for H_2 production.[9] Also, mononuclear complexes such as iron[10] and rhodium[11] porphyrins, and cobalt[11] and nickel[12] complexes have been reported and aspects of these catalysts have been reviewed.[13]

This paper is concerned with the formation of molecular hydrogen from the mononuclear iron complex $(\eta^5\text{-}C_5H_5)Fe(CO)_2H$ (FpH) and development of a catalytic system for generating H_2. FpH has been reported[14] to spontaneously decompose into Fp_2 and H_2. However, this reaction is apparently a chain process initiated by adventitious oxidants and inhibited by a variety of additives.[15] Furthermore, FpH is stable to acetic acid. We have recently reported[16] that, although the μ-hydride monoanion **1** is stable to acetic acid, on reduction it forms a dianion which reacts with acetic acid, generating H_2. Thus, the μ-hydride monoanion **1** is a weaker hydride donor than its more electron-rich corresponding dianion. Consequently, it was

* To whom correspondence should be addressed. E-mail: dlichten@email.arizona.edu.

(1) Navarro, R. M.; Pena, M. A.; Fierro, J. L. G. *Chem. Rev.* **2007**, *107*, 3952–3991.

(2) Elvington, M.; Brown, J.; Arachchige, S. M.; Brewer, K. J. *J. Am. Chem. Soc.* **2007**, *129*, 10644–10645.

(3) (a) Hahn, J.-J.; Ghirardi, M. L.; Jacoby, W. A. *Biochem. Eng. J.* **2007**, *37*, 75–79. (b) Rey, F. E.; Heiniger, E. K.; Harwood, C. S. *Appl. Environ. Microbiol.* **2007**, 1665–1671. (c) Prince, R. C.; Keshgi, H. S. *Crit. Rev. Microbiol.* **2005**, *31*, 19–31.

(4) Vincent, K. A.; Parkin, A.; Armstrong, F. A. *Chem. Rev.* **2007**, *107*, 4366–4413.

(5) (a) Lyon, E. J.; Shima, S.; Buurman, G.; Chowdhuri, S.; Batschauer, A.; Steinbach, K.; Thauer, R. K.; Grevels, F.-W.; Albracht, S. R. J. *J. Am. Chem. Soc.* **2004**, *126*, 14239–14248. (b) Shima, S.; Lyon, E. J.; Sordel-Klippert, M.; Kauss, M.; Kahnt, J.; Thauer, R. K.; Steinbach, K.; Xie, X.; Verdier, L.; Griesinger, C. *Angew. Chem., Int. Ed.* **2004**, *43*, 2547–2551. (c) Shima, S.; Thauer, R. K. *Chem. Rec.* **2007**, *7*, 37–46.

(6) (a) Vignais, P. M.; Billoud, B. *Chem. Rev.* **2007**, *107*, 4206–4272. (b) Fontecilla-Camps, J. C.; Volbeda, A.; Cavazza, C.; Nicolet, Y. *Chem. Rev.* **2007**, *107*, 4273–4303.

(7) (a) Perra, A.; Davies, E. S.; Hyde, J. R.; Wang, Q.; McMaster, J.; Schröder, M. *Chem. Commun.* **2006**, 1103–1105. (b) Oudart, Y.; Artera, V.; Pècaut, J.; Fontecave, M. *Inorg. Chem.* **2006**, *45*, 4334–4336. (c) Orgo, S.; Kabe, R.; Uehara, K.; Kure, B.; Nishimura, T.; Menon, S. C.; Harada, R.; Fukuzumi, S.; Higuchi, Y.; Ohhara, T.; Tamada, T.; Kuroki, R. *Science* **2007**, *316*, 585–587.

10.1021/om800366h CCC: $40.75
Publication on Web 08/21/2008

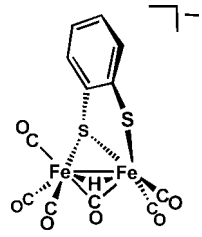

1

surmised that reduction of FpH would increase its hydridicity,[17] enabling its reaction with weak acids to form H_2. Since Fp_2 is known to undergo two-electron reduction at an electrode to form Fp^-, subsequent protonation provides a convenient electrochemical synthesis of FpH.[18]

Scheme 1. Fp_2 Reduction Followed by Catalytic Reduction of Protons to H_2

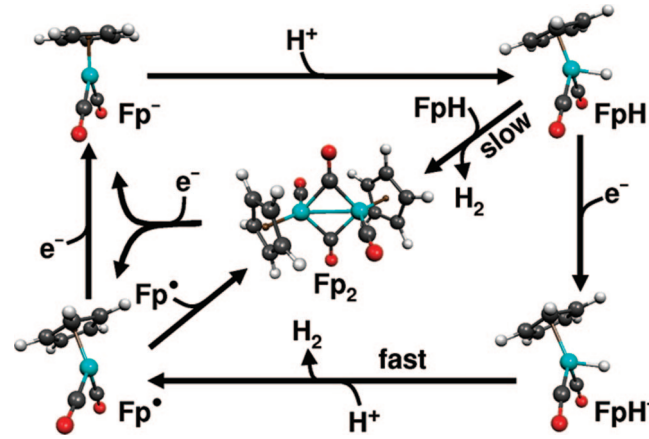

Through a series of electrochemical and redox equilibrium measurements, Pugh and Meyer[18,19] were able to establish that $E° = -1.44$ V vs an aqueous saturated sodium chloride calomel electrode (ca. -1.84 V vs ferrocene in acetonitrile[20]) for the redox couple $Fp_2 + 2e^- \rightleftharpoons 2Fp^-$. Many acids could be used for protonating Fp^-, since the pK_a value of FpH has been reported to be 19.4.[21]

This paper reports the formation of Fp^- by electrochemical reduction of Fp_2, and upon addition of various weak acids, the hydride is formed, which undergoes further reduction at more negative potentials, initiating a catalytic cycle leading to the generation of dihydrogen. Fp_2 is known to exist predominantly as a set of two CO-bridged isomers, *cis*- and *trans*-[(η^5-C_5H_5)Fe(μ-CO)(CO)]$_2$,[22] but the effects of such isomerism were not apparent in our experiments. Though oxidation of (η^5-C_5H_5)Fe(CO)$_2^-$ (Fp^-) has been studied,[18,23] we are not aware of electrochemical studies of the oxidation of (η^5-C_5H_5)Fe(CO)$_2$H (FpH), which are reported here along with the aforementioned catalytic reductive process. To aid in the interpretation of our results, we have conducted extensive theoretical studies of Fp_2, Fp^-, FpH and related species in the catalytic cycle (calculating $E°$ and pK_a values as well as infrared spectra and ionization energies) and the theoretical methods have been validated by comparison with our experimental results and results from the literature.

Results

The reactions to be discussed in this work are shown in Scheme 1 along with depictions of the computed structures of Fp_2 and various species involved in the catalyzed reduction of acid. Fp_2 is located in the center of the diagram, and the reactions involved in its reduction to Fp^- are on the left-hand side. The rest of the reactions pertain to the catalyzed reduction of a proton source to form dihydrogen. The results of a study of the reduction of Fp_2 will be presented first, followed by studies of the mechanism of the catalytic reduction of weak acids. The

(8) (a) Darensbourg, M. Y.; Lyon, E. K.; Smee, J. J. *Coord. Chem. Rev.* **2000**, *206−207*, 533–561. (b) King, R. B.; Bitterwolf, T. E. *Coord. Chem. Rev.* **2000**, *206−207*, 563–279. (c) Darensbourg, M. Y.; Lyon, E. J.; Zharo, X.; Georgkaki, I. P. *Proc. Natl. Acad. Sci. U.S.A.* **2003**, *100*, 3683–3688. (d) Georgkaki, I. P.; Thomson, L. M.; Lyon, E. J.; Hamm, M. B.; Darensbourg, M. Y. *Coord. Chem. Rev.* **2003**, *238−239*, 255–266. (e) Evans, D. J.; Pickett, C. J. *Chem. Soc. Rev.* **2003**, *32*, 268–275. (f) Liu, X.; Ibrahim, S. K.; Pickett, C. J. *Chem. Soc. Rev.* **2005**, *249*, 1641–1652. (g) Tard, C.; Liu, X.; Ibrahim, S. K.; Bruschi, M.; De Gioia, L.; Davies, S. C.; Yang, X.; Wang, L.-S.; Sawers, G.; Pickett, C. J. *Nature* **2005**, *433*, 610–613. (h) Sun, L.; Akermark, B.; Ott, S. *Coord. Chem. Rev.* **2005**, *249*, 1653–1663. (i) van der Vlugt, J. I.; Rauchfuss, T. B.; Wilson, S. T. *Chem. Eur. J.* **2006**, *12*, 90–98. (j) Linck, R. C.; Rauchfuss, T. B. In *Bioorganometallics Biomolecules, Labeling, Medicine*; Jaouen, G., Ed.; Wiley-VCH: Weinheim, Germany, 2006; Chapter 12. (k) Song, L.-C.; Ge, J.-H.; Zhang, X.-G.; Liu, Y.; Hu, Q.-M. *Eur. J. Inorg. Chem.* **2006**, 3204–3210. (l) Schwartz, L.; Ekström, J.; Lomoth, R.; Ott, S. *Chem. Commun.* **2006**, 4206–4208. (m) Gao, W.; Ekström, J.; Liu, J.; Chen, C.; Eriksson, L.; Weng, L.; Akermark, B.; Sun, L. *Inorg. Chem.* **2007**, *46*, 1981–1991. (n) Wang, Z.; Liu, J.; He, C.; Jiang, S.; Akermark, B.; Sun, L. *Inorg. Chim. Acta* **2007**, *360*, 2411–2419. (o) Jiang, S.; Liu, J.; Shi, Y.; Wang, Z.; Akermark, B.; Sun, L. *Polyhedron* **2007**, *26*, 1499–1504. (p) Jiang, S.; Liu, J.; Shi, Y.; Wang, Z.; Akermark, B.; Sun, L. *Dalton Trans.* **2007**, 896–902. (q) Duan, L.; Wang, M.; Li, P.; Na, Y.; Wang, N.; Sun, L. *Dalton Trans.* **2007**, 1277–1283.

(9) Appel, A. M.; DuBois, D. L.; Rakowski DuBois, M. *J. Am. Chem. Soc.* **2005**, *127*, 12717–12726.

(10) Bhugun, I.; Lexa, D.; Saveant, J. *J. Am. Chem. Soc.* **1997**, *118*, 3982–3983.

(11) (a) Razavet, M.; Artero, V.; Fontecave, M. *Inorg. Chem.* **2005**, *44*, 4786–4795. (b) Hu, X.; Cossairt, B. M.; Brunschwig, B. S.; Lewis, N. S.; Peters, J. C. *Chem. Commun.* **2005**, 4723–4725. (c) Baffert, C.; Artero, V.; Fontecave, M. *Inorg. Chem.* **2007**, *46*, 3502–3510. (d) Hu, X.; Brunschwig, B. S.; Peters, J. C. *J. Am. Chem. Soc.* **2007**, *129*, 8988–8998.

(12) (a) Lee, C.-M.; Chuang, Y.-L.; Chiang, C.-Y.; Lee, G.-H.; Liaw, W.-F. *Inorg. Chem.* **2006**, *45*, 10895–10904. (b) Fraze, K.; Wilson, A. D.; Appel, A. M.; Rakowski DuBois, M.; Dubois, D. L. *Organometallics* **2007**, *26*, 3918–3924. (c) Wilson, A. D.; Shoemaker, R. K.; Miedaner, A.; Muckerman, J. T.; DuBois, D. L.; DuBois, M. R. *Proc. Natl. Acad. Sci. USA* **2007**, *104*, 6951–6956.

(13) Artero, V.; Fontecave, M. *Coord. Chem. Rev.* **2005**, *249*, 1518–1535.

(14) Green, M. L. H.; Street, C. N.; Wilkinson, G. Z. *Naturforsch.* **1959**, *14B*, 738.

(15) (a) Fergusson, S. B.; Sanderson, L. J.; Shackleton, T. A.; Baird, M. C. *Inorg. Chim. Acta* **1984**, *83*, L45–L47. (b) Shackleton, T. A.; Mackie, S. C.; Fergusson, S. B.; Johnston, L. V.; Baird, M. C. *Organometallics* **1990**, *9*, 2248–2253.

(16) Felton, G. A. N.; Vannucci, A. K.; Chen, J.; Lockett, L. T.; Okumura, N.; Petro, B. J.; Zakai, U. I.; Evans, D. H.; Glass, R. S.; Lichtenberger, D. L. *J. Am. Chem. Soc.* **2007**, *129*, 12521–12530.

(17) (a) Jacobsen, H.; Berke, H. In *Recent Advances in Hydride Chemistry*; Peruzzini, M., Poli, R., Eds.; Elsevier: Amsterdam, 2001; Chapter 4. (b) Curtis, C. J.; Miedaner, A.; Ellis, W. W.; DuBois, D. L. *J. Am. Chem. Soc.* **2002**, *124*, 1918–1925.

(18) (a) Dessey, R. E.; Stary, F. E.; King, R. B.; Waldrop, M. *J. Am. Chem. Soc.* **1966**, *88*, 471–476. (b) Miholová, D.; Vlček, A. A. *Inorg. Chim. Acta* **1980**, *41*, 119–122. (c) Davies, S. G.; Simpson, S. J.; Parker, V. D. *J. Chem. Soc., Chem. Commun.* **1984**, 352–353. (d) Dalton, E. F.; Ching, S.; Murray, R. W. *Inorg. Chem.* **1991**, *30*, 2642–2648. (e) Pugh, J. R.; Meyer, T. J. *J. Am. Chem. Soc.* **1992**, *114*, 3784–3792. (f) Fukuzumi, S.; Ohkubo, K.; Fujitsuka, M.; Ito, O.; Teichmann, M. C.; Maisonhaute, E.; Amatore, C. *Inorg. Chem.* **2001**, *40*, 1213–1219.

(19) Pugh, J. R.; Meyer, T. J. *J. Am. Chem. Soc.* **1988**, *110*, 8245–8246.

(20) Shalev, H.; Evans, D. H. *J. Am. Chem. Soc.* **1989**, *111*, 2667–2674.

(21) Moore, E. J.; Sullivan, J. M.; Norton, J. R. *J. Am. Chem. Soc.* **1986**, *108*, 2257–2263.

(22) (a) For a discussion of solid-state isomerism and references to earlier solution-phase experiments, see ref 22b. (b) Braga, D.; Chierotti, M. R.; Garino, N.; Gobetto, R.; Grepioni, F.; Polito, M.; Viale, A. *Organometallics* **2007**, *26*, 2266–2271.

(23) Tilset, M.; Parker, V. D. *J. Am. Chem. Soc.* **1989**, *111*, 6711–6717.

Table 1. Reaction Steps, Parameters, and Parameter Values for Simulation of Electrochemical Results for Fp_2 in the Absence and Presence of 4-*tert*-Butylphenol[a]

reaction no.	reaction	parameters
2	$Fp_2 + e^- \rightleftharpoons Fp_2^{\bullet -}$	E°_2, $k_{s,2}$, α_2
3	$Fp_2^{\bullet -} \rightleftharpoons Fp^\bullet + Fp^-$	K_3, $k_{f,3}$, $k_{b,3}$
4	$Fp^\bullet + e^- \rightleftharpoons Fp^-$	E°_4, $k_{s,4}$, α_4
5	$2Fp^\bullet \rightleftharpoons Fp_2$	K_5, $k_{f,5}$, $k_{b,5}$
6	$Fp^- + HA \rightleftharpoons FpH + A^-$	K_6, $k_{f,6}$, $k_{b,6}$
7	$FpH + e^- \rightleftharpoons FpH^{\bullet -}$	E°_7, $k_{s,7}$, α_7
8	$FpH^{\bullet -} + HA \rightleftharpoons FpH \cdot HA^{\bullet -}$	K_8, $k_{f,8}$, $k_{b,8}$
9	$FpH \cdot HA^{\bullet -} \rightleftharpoons FpHH^\bullet + A^-$	K_9, $k_{f,9}$, $k_{b,9}$
10	$FpHH^\bullet \rightleftharpoons Fp^\bullet + H_2$	K_{10}, $k_{f,10}$, $k_{b,10}$
11	$HA + A^- \rightleftharpoons HA_2^-$	K_{11}, $k_{f,11}$, $k_{b,11}$
12	"FpHg" $+ e^- \rightleftharpoons Fp^-$	E°_{12}, $k_{s,12}$, α_{12}

reaction no.	reaction	E°/V	k_s/cm s^{-1}	α
2	$Fp_2 + e^- \rightleftharpoons Fp_2^{\bullet -}$	−2.034	2.2	0.5
4	$Fp^\bullet + e^- \rightleftharpoons Fp^-$	−1.409	0.05	0.5
7	$FpH + e^- \rightleftharpoons FpH^{\bullet -}$	−2.589	0.01	0.5
12[b]	"FpHg" $+ e^- \rightleftharpoons Fp^-$	−1.682	0.1	0.999

reaction no.	reaction	K	k_f	k_b
3	$Fp_2^{\bullet -} \rightleftharpoons Fp^\bullet + Fp^-$	10	1.0×10^4	1.0×10^3
5	$2Fp^\bullet \rightleftharpoons Fp_2$	3.65×10^9	1.0×10^8	2.74×10^{-2}
6	$Fp^- + HA \rightleftharpoons FpH + A^-$	0.03	1.0×10^5	3.33×10^6
8	$FpH^{\bullet -} + HA \rightleftharpoons FpH \cdot HA^{\bullet -}$	1.0×10^3	1.0×10^8	1.0×10^5
9	$FpH^{\bullet -} + HA \rightleftharpoons FpH \cdot HA^{\bullet -}$	6.3×10^{-5}	1.0×10^4	1.58×10^8
10	$FpHH^\bullet \rightleftharpoons Fp^\bullet + H_2$	1.0×10^5	1.0×10^3	1.0×10^{-2}
11	$HA + A^- \rightleftharpoons HA_2^-$	1.58×10^4	1.0×10^8	6.33×10^3

[a] Simulations are as shown in Figures 1 and 2. That is, the acid in the acid-dependent reactions (reactions 6, 8, 9, and 11) is 4-*tert*-butylphenol (HA). The parameter values for reaction 6 were established by simulation of voltammograms of Fp_2 in the presence of HA that included only the first reduction peak and the oxidation peak, such as Figure 1B. E°_i, $k_{s,i}$ and α_i are the standard potential (V vs ferrocene), standard rate constant (cm/s), and electron transfer coefficient of electrode reaction *i*. K_j, $k_{f,j}$ and $k_{b,j}$ are the equilibrium constant, forward rate constant, and reverse rate constant of chemical reaction *j*. Units of rate constants of chemical reactions: s^{-1} for first-order reactions and M^{-1} s^{-1} for second-order reactions. Electrode areas are given in the Experimental Section. Diffusion coefficients: Fp_2 and $Fp_2^{\bullet -}$, 1.7×10^{-5} cm^2/s; $Fp^\bullet$, Fp^-, 2.0×10^{-5} cm^2/s; "FpHg", 1.0×10^{-5} cm^2/s. We could find no evidence for the intermediate "$FpHH^\bullet$" by computation. The overall reaction $FpH^{\bullet -} + HA \rightleftharpoons Fp^\bullet + H_2 + A^-$ was treated as three fast sequential reactions, reactions 8−10, due to software limitations in the commercial simulation program. Homoconjugation reaction 11 was assigned an equilibrium constant equal to that reported[26b] for phenol, $10^{4.2}$. [b] The oxidation of mercury in the presence of Fp^- is complex, as mentioned in the text. The reaction proceeds to a mixture of $(Fp)_2Hg$ and $(Fp)_3Hg^-$, depending on conditions, and the composition of the mixture may vary in different portions of the diffusion layer and at various points on the voltammogram. This complex reaction was mimicked by the reaction shown as 12, whose parameter values should not be regarded as significant.

reactions in Scheme 1 will be recast in normal linear form for purposes of the presentation and discussion of the results (reactions 2−12 in Table 1).

Reduction of Fp_2 in the Absence of Added Acid. Figure 1 shows two voltammograms of Fp_2 obtained in acetonitrile/0.10 M Bu_4NPF_6 at (A) a glassy-carbon electrode and (B) a mercury-film working electrode. Each voltammogram shows an irreversible two-electron-reduction peak and an oxidation peak at a less negative potential on the return cycle. The reduction process comprises reactions 2−4 at both electrodes. On glassy carbon, Fp^-, produced at the cathodic peak, is oxidized by the reverse of reaction 4, giving the neutral radical that rapidly dimerizes[24] to Fp_2 (reaction 5), thus accounting for the lack of reversibility as revealed by a second scan cycle (not shown). In contrast, on mercury the oxidation proceeds with incorporation of mercury to produce mixtures of $[(\eta^5\text{-}C_5H_5)Fe(CO)_2]_2Hg$ and $[(\eta^5\text{-}C_5H_5)Fe(CO)_2]_3Hg^-$, as determined in an earlier study.[18] This anodic reaction is reversible, as indicated by the reduction peak seen on the negative portion of the second cycle (Figure 1B).

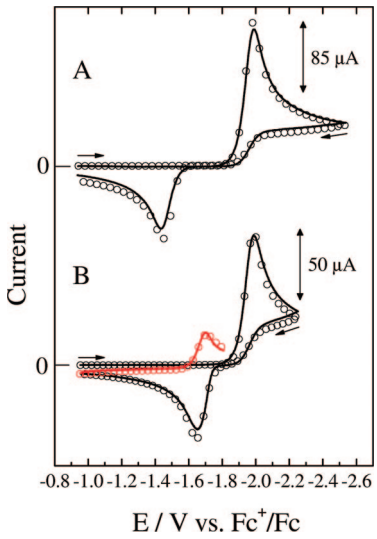

Figure 1. Voltammograms of Fp_2 in the absence of added acid (0.10 M Bu_4NPF_6, acetonitrile, 0.100 V/s): (A) glassy-carbon electrode, 1.04 mM Fp_2; (B) mercury-film electrode, 1.05 mM Fp_2. The third half-cycle is shown in red, and the area is 0.12 cm^2. The solid lines denote the background-corrected experimental voltammograms, and the open circles are simulations using parameter values given in Table 1.

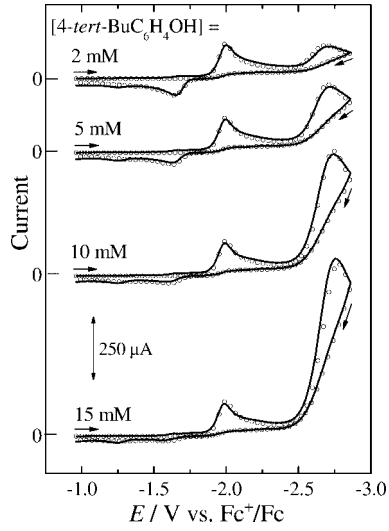

Figure 2. Voltammograms of 0.50 mM Fp_2 in the presence of 4-*tert*-butylphenol at the concentrations specified (mercury-film electrode (0.0123 cm^2), 0.10 M Bu_4NPF_6, acetonitrile, 1.00 V/s). Solid lines denote background-corrected experimental voltammograms, and the open circles denote simulations using parameter values given in Table 1.

The points in Figure 1 correspond to simulations based on reactions 2−5 (for glassy carbon) and reactions 2−5 and 12 for mercury. Reaction 12, "FpHg" + $e^- \rightleftharpoons Fp^-$, is used as a simple mimic of the complex chemistry leading to the soluble mercury complexes mentioned above. The simulation parameter values that were used are given in Table 1. These same parameters were found to fit data obtained at 0.1, 0.5, 1, 3, and 5 V/s (glassy carbon), 0.1, 0.5, and 1 V/s (two-cycle data with Hg film), and 0.5, 1, 2, and 3 V/s (single-cycle data with Hg film).

(24) Caspar, J. V.; Meyer, T. J. *J. Am. Chem. Soc.* **1980**, *102*, 7794–7795.

Reduction of Fp_2 in the Presence of Acid. Preparation of FpH. Controlled-potential reduction of 0.50 mM Fp_2 at a platinum electrode in acetonitrile was confirmed to require two electrons per molecule of Fp_2, and the electrolyzed solution showed the characteristic oxidation peak for Fp^- (as in Figure 1A), consistent with the overall stoichiometry obtained from the sum of reactions 2−4, $Fp_2 + 2e^- \rightarrow 2Fp^-$. The reported[21] pK_a value of FpH is 19.4, indicating that an appropriate acid should be able to protonate the Fp^- that is produced in the electrolysis. When 1 mM Fp_2 was electrolyzed at a mercury pool electrode at −2.26 V in acetonitrile containing 2 mM acetic acid, 1.8 electrons per molecule of Fp_2 were required. The mercury electrode was used to prevent the direct electrochemical reduction of the acid, which would interfere if a platinum or glassy-carbon electrode were used.[25] The electrolyzed solution was examined by voltammetry with a mercury film electrode, and an irreversible reduction peak, assigned to FpH, was seen at −2.54 V (0.10 V/s). There was also a very small peak for oxidation of Fp^-, like that in Figure 1B. In a separate experiment, electrolysis (−2.36 V) of 0.52 mM Fp_2 at a platinum electrode was conducted to 79% completion to produce a solution of Fp^-. Then 1 mM acetic acid was added, and voltammetry with a glassy-carbon electrode revealed an irreversible anodic peak at +0.60 V, which we assign to oxidation of FpH. Thus, reduction of Fp_2 in the presence of acetic acid results in the production of FpH according to reaction 13.

$$Fp_2 + 2CH_3COOH + 2e^- \rightleftharpoons 2FpH + 2CH_3CO_2^- \quad (13)$$

This observation is somewhat surprising, as the pK_a of acetic acid is 22.3 in acetonitrile,[26] indicating that this acid should be far too weak to protonate Fp^-. This point will be discussed later.

As mentioned in the Introduction, it is well-known that FpH can react to give Fp_2 and H_2. If this reaction occurred to a significant extent during the electrolysis in the presence of acid, the Fp_2 so generated would be reduced at the electrode to Fp^-, requiring more reductive electrical charge to complete the electrolysis. In fact, the charge during the electrolysis, which required ca. 30 min, did not exceed two electrons per molecule of Fp_2 (one per molecule of CH_3COOH), as indicated by reaction 13. Therefore, reaction of FpH to give Fp_2 and H_2 does not occur rapidly enough to be a significant path for the catalytic reduction of acetic acid under these conditions. One reason for the slowness of reaction 1 may be the low concentrations that were used. In separate experiments with the aim of preparing pure samples of FpH, we have found that evaporating the solvent in order to obtain concentrated solutions leads to rapid evolution of H_2 with formation of Fp_2.

Reduction of Fp_2 in the Presence of Excess Acid. Catalytic Reduction of Acid To Form H_2. Having established that no significant catalytic hydrogen production occurs during electrolysis of Fp_2 in the presence of a stoichiometric amount of acetic acid under these conditions, the behavior in the presence of excess acid was then explored. When studied by voltammetry, the reduction peak for Fp_2 does not increase in height even in the presence of a hundred-fold excess of acetic acid. Thus, it is clear that the catalytic cycle involving reaction 13, followed by $2FpH \rightarrow Fp_2 + H_2$, does not occur to a significant extent on the voltammetric time scale because the regeneration of Fp_2 would have produced more current at the potential of its

(25) Felton, G. A. N.; Glass, R. S.; Lichtenberger, D. L.; Evans, D. H. *Inorg. Chem.* **2006**, *45*, 9181–9184.

(26) (a) Unless otherwise stated, all pK_a values are from ref 26b. (b) Izutsu, K. *Acid-Base Dissociation Constants in Dipolar Aprotic Solvents*; Blackwell Scientific: Oxford, U.K., 1990.

reduction. When acids stronger than acetic acid, *p*-toluenesulfonic acid (pK_a = 8.73) and trifluoroacetic acid (pK_a = 12.65), were studied, the solution of Fp_2 became light yellow and new reduction peaks appeared in the range of −0.9 to −1.5 V, which were not observed when acetic acid was present. However, there was no increase in current at the main peak for Fp_2 reduction. In fact, this peak decreased in magnitude, as though Fp_2 was being converted to species that are reducible at potentials less negative than for Fp_2. One possibility is the protonated Fp_2 species reported by Legzdins et al.[27] which was formed when Fp_2 was treated with $HBF_4 \cdot OMe_2$. The behavior of Fp_2 in the presence of strong acids was not studied further.

Nevertheless, efficient catalysis does occur, even with acids much weaker than acetic acid. The catalytic process simply occurs at a more negative potential, as illustrated in Figure 2. Here an acid even weaker than acetic acid, 4-*tert*-butylphenol (pK_a = 27.5), has been added to a 0.50 mM solution of Fp_2 using a mercury-film electrode for the voltammetry in order to avoid direct reduction of the acid that tends to occur at glassy carbon.[25] The initial negative scan shows the reduction peak for Fp_2 that was discussed above. With 2 mM acid, a significant reduction peak appears near −2.7 V, the peak assigned earlier to the reduction of FpH. This is due to the fact that even the much weaker acid, 4-*tert*-butylphenol, is able to protonate a significant fraction of the Fp^- formed in the first peak, allowing the peak for reduction of FpH to appear.

This peak grows as the concentration of acid is increased (Figure 2). That this peak is more than simply the reduction of FpH formed at the first peak is indicated by the fact that its height continues to grow with increasing acid concentration (as large as 100 mM,; data not shown). The most reasonable interpretation is that FpH participates in a catalytic cycle that results in the reduction of the acid to dihydrogen and the conjugate base. The proposed reaction cycle comprises reactions 4 and 6−10. The simulations included in Figure 2 were carried out with the parameters listed in Table 1. The simulation parameter values for reactions 2−4 and 12 are the same as those used to fit the voltammograms for reduction of Fp_2 in the absence of acid (Figure 1). Reaction 6 is the rate-determining step (rds) with 8−10 treated as fast reactions following the rds. With 4-*tert*-butylphenol as proton donor, reaction 6 is not favored, $K_6 = 0.03$ being established with considerable accuracy by simulations of voltammograms of Fp_2 in the presence of acid but for a potential window that includes only the first reduction and oxidation peak, as in Figure 1. This value of the equilibrium constant of reaction 6 can be incorporated with the pK_a of 4-*tert*-butylphenol (27.5) to give $pK_a = 26.0$ for FpH, which is much larger than the earlier experimental value[21] of 19.4. Simulations of other scan rates and acid concentrations, one other Fp_2 concentration, and a discussion of the reactions used in the mechanism are presented in the Supporting Information. It is important to note that the same simulation parameter values were successful in matching the data at all scan rates and acid concentrations and the two Fp_2 concentrations that were studied (0.5 mM Fp_2 with 0, 2, 5, 10, and 15 mM 4-*tert*-butylphenol (0.5, 1, 2, and 3 V/s), and 1 mM Fp_2 with 0, 2, 5, 10, and 20 mM 4-*tert*-butylphenol (0.5, 1, and 2 V/s)).

At this point, the inconsistency between the reported pK_a for FpH of 19.4 and that determined by our electrochemical studies (∼26) was addressed. Calculations support FpH being a weaker acid than that reported with a calculated pK_a of 28.3. Hence, a reinvestigation of the pK_a by infrared absorbance studies was carried out. A 1:1 mixture of Fp^- and 4-*tert*-butylphenol resulted in near equal concentrations of Fp^- and FpH at equilibrium (spectrum in the Supporting Information), indicating that the pK_a of FpH must be near the pK_a of 4-*tert*-butylphenol (27.5).

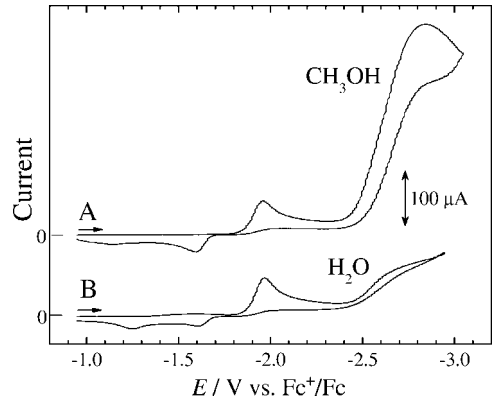

Figure 3. Background-corrected voltammograms of Fp_2 in the presence of methanol and water (0.10 M Bu_4NPF_6 in acetonitrile, mercury-film electrode, 0.100 V/s): (A) 1.015 mM Fp_2 with 3.26 M methanol; (B) 1.005 mM Fp_2 with 4.12 M water.

Using the half-peak potential of the catalytic peak in Figure 2 (ca. −2.6 V) as the potential for catalytic reduction of 4-*tert*-butylphenol and comparing this with the standard potential[25] for reduction of 4-*tert*-butylphenol in acetonitrile, −1.77 V, it may be seen that the process is occurring with 0.8 V overpotential. Thus, by this measure of efficiency, Fp_2 is not a promising catalyst.

However, 4-*tert*-butylphenol is the weakest acid that has been shown to undergo significant catalyzed reduction using transition-metal complexes as catalysts. In our previous study[16] using [(μ-1,2-benzenedithiolato)][$Fe(CO)_3$]$_2$ as catalyst, no detectable catalytic current was seen with 4-*tert*-butylphenol, somewhat stronger acids such as 4-bromophenol (pK_a = 25.5) being necessary for appreciable catalytic reduction. To see how effective Fp_2 might be with still weaker acids, experiments were conducted in the presence of the much weaker acids: methanol and water.[28] Very weak but readily detectable catalytic reduction was seen, as illustrated in Figure 3 for 3.26 M methanol and 4.12 M water. Interestingly, the catalysis occurs at potentials in the vicinity of −2.6 to −2.8 V, just as seen in Figure 2, because the potential is principally governed by $E°_7$, which is independent of the acid used. Since the potential required for the catalysis is more or less constant, the overpotential with these much weaker acids is considerably lower. This illustrates a trend noted earlier:[16] when a series of acids with varying acid strengths are studied, the lowest overpotentials are associated with smallest catalytic currents.

Turning to stronger acids, Figure 4 shows the results for 4-*tert*-butylphenol (pK_a = 27.5), 4-bromophenol (pK_a = 25.5),

(27) Legzdins, P.; Martin, D. T.; Nurse, C. R.; Wassink, B. *Organometallics* **1983**, *2*, 1238–1244.

(28) We have not located pK_a values for methanol and water in acetonitrile. Estimates can be based on comparison of the pK_a values of various other oxygen acids in acetonitrile and DMSO. On average, the values are 10 units higher in acetonitrile, and this quantity can be added to the pK_a of methanol in DMSO (28.99[26b]) and that of water in DMSO (28.2, 31.36[26b]). These very large estimated values of pK_a (39 and 38−41, respectively) in acetonitrile may not be significant as they exceed the estimated negative logarithm of the autoprotolysis constant of the solvent, 28.6, 33.2 or 33.3.[26b] (see, however:Schwesinger, R.; Schlemper, H. *Angew. Chem., Int. Ed. Engl.* **1987**, *26*, 1167-1169, where the pK_a of acetonitrile is estimated as >44). In any case, methanol and water act as extremely weak acids in acetonitrile. Furthermore, attempts to simulate the data in Figure 3 using the mechanism found for 4-*tert*-butylphenol were unsuccessful using these very large values of pK_a for water and methanol. Values in the range pK_a = 33−35 were necessary to simulate the observed currents.

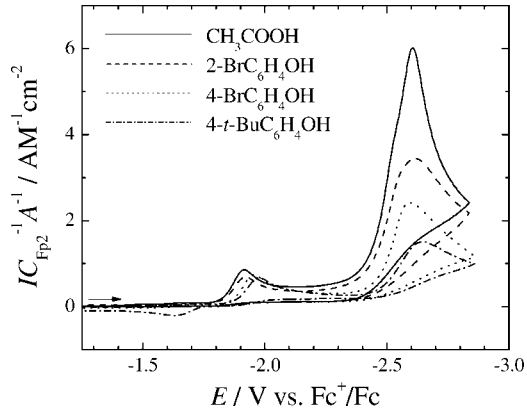

Figure 4. Background-corrected voltammograms of Fp_2 in the presence of 10.0 mM concentrations of four acids (0.10 M Bu_4NPF_6 in acetonitrile, mercury-film electrode, 0.100 V/s). The ordinate has been normalized for the slightly variant concentrations of Fp_2 (all near 1 mM) and the slightly variant electrode area (all near 0.12 cm_2). pK_a values:[26b] acetic acid, 22.3; 2-bromophenol, 23.9; 4-bromophenol, 25.5; 4-*tert*-butylphenol, 27.5.

2-bromophenol (pK_a = 23.9) and acetic acid (pK_a = 22.3). The results in Figure 4 reveal that the catalytic current increases as the acids become stronger. This is mainly due to the change in K_6, which increases from 0.03 for 4-*tert*-butylphenol (as determined by the simulations just discussed) to values of 3, 120, and 4700 for the three remaining acids, respectively. Thus, the equilibrium constant in the rate-determining step increases with the acid dissociation constant, thus favoring the catalysis.

Parameter values for reactions 2−4 and 12 have been determined by simulation of voltammograms obtained in the absence of acid (see above and Table 1). In addition, parameter values for reaction 6 were evaluated by studies of the first reduction and sole oxidation peak in the presence of the three stronger acids. The homoconjugation constants (reaction 11) were maintained at 1.58×10^4 M^{-1} for the phenols (the value for phenol itself[26]), and that for acetic acid, 6000 M^{-1}, was taken from the literature.[26] Examples of the fits of simulation to background-corrected voltammograms are included in the Supporting Information.

Simulations of the complete voltammograms, including the catalytic peak, were successful for 4-bromophenol using the same mechanism as that for 4-*tert*-butylphenol, and the relevant reactions and the simulation parameter values are given in Table 2. Examples of fits of simulations to background-corrected voltammograms for 4-bromophenol are included in the Supporting Information.

Simulations of the catalytic peaks of 2-bromophenol and acetic acid were qualitatively consistent with the larger values of K_6 mentioned above, although the overall simulations were not as quantitatively successful. It is suspected that the increase in the effective rate of reaction 6 brings about a transfer of the rate-determining step to reactions 8−10.

Defining the overpotential as the difference between the standard potential for acid reduction and the half-peak potential of the catalytic peak gives values of 0.77 V for 4-*tert*-butylphenol, 0.87 V for 4-bromophenol, 0.94 V for 2-bromophenol, and 1.04 V for acetic acid (data taken from Figure 4). This is another vivid demonstration of the earlier observed trend[16] with [(μ-1,2-benzenedithiolato)][$Fe(CO)_3$]$_2$ as catalyst: lower overpotentials (desired) correlate with lower catalytic currents (undesired).

Computations. The results for the computed gas-phase structure of Fp_2 are shown in Table 3 in comparison to the structure determined from X-ray crystallography.[29] The computed and experimental structural parameters are in close agreement. In addition to the ability of the calculations to account for the molecular geometries, it is important for the calculations to account for the energies of the species involved in the catalytic cycle. Photoelectron spectroscopy is a well-defined method for determining electron energies by measuring ionization energies of molecules in the gas phase and, hence, provides a good benchmark for calculated gas-phase energies. Figure 5 shows the photoelectron spectra of FpH (A) and Fp_2 (B). These spectra compare favorably with the spectra of FpH[30,31] and Fp_2[32,33] reported previously. The purpose for recollecting these photoelectron spectra was not to assign the individual ionizations but to illustrate comparison of the ionizations obtained with accurate energy calibration with the results of calculations. The arrows at low energy on each spectrum indicate the calculated adiabatic ionization energy, which is the difference in energy of the ground-state neutral molecule and the geometry-relaxed cation. For larger molecules such as Fp_2, the first ionization peak is not vibrationally resolved and the adiabatic ionization energy is estimated by the low-energy onset of ionization intensity. The arrows at higher energy on each spectrum point to the calculated vertical ionization, which is the energy difference between the ground-state neutral molecule and the cation molecule frozen in the optimized geometry of the neutral molecule. As can be seen in Figure 5, the calculated adiabatic (7.76 eV for FpH and 6.80 eV for Fp_2) and vertical ionization energies (8.23 eV for FpH and 6.98 eV for Fp_2) are in excellent agreement with the experimentally observed ionization bands.

In addition, computed and experimental carbonyl stretching frequencies in the infrared spectra of Fp_2, Fp^-, and FpH are shown in Figure 6. Again, it may be seen that excellent agreement is obtained between the computed and experimental infrared frequencies and intensities. This is additional evidence that the calculations account well for the structures and electron richness of the molecules and the potential energy surfaces in the regions of the optimum geometries.

The calculations are also able to account for the solution-phase oxidation and reduction of the species involved in the catalytic cycle. For the case of oxidation, it has been reported that the standard potential for $Fp_2^{\bullet+} + e^- \rightleftharpoons Fp_2$ is +0.22 V in dichloromethane.[34] Our calculations are in very good agreement, resulting in a value of +0.21 V. We were unable to obtain the experimental reversible potential for oxidizing FpH ($FpH^{\bullet+} + e^- \rightleftharpoons$ FpH) for proper comparison with the calculations. However, the *irreversible* oxidation of FpH in acetonitrile is +0.60 V, which is reasonable in comparison to the value of +0.72 V for the standard potential obtained through calculations.

The calculations also account well for the reduction of Fp_2 in acetonitrile. The standard potential for reduction of Fp_2, $E°_2$, is −2.035 V, as estimated by simulation, whereas the calculated value is −2.055 V. The calculated standard potential for reduction of $Fp^{\bullet}$, $E°_4$, is −1.01 V, which cannot be obtained from simulations of the electrochemical data because the

(29) Mitschler, A.; Rees, B.; Lehmann, M. S. *J. Am. Chem. Soc.* **1978**, *100*, 3390–3397.
(30) Renshaw, S. K. *Diss. Abstr. Int. B* **1992**, *52*, 5259.
(31) Lichtenberger, D. L.; Gruhn, N. E.; Renshaw, S. K. *J. Mol. Struct.* **1997**, *405*, 79–86.
(32) Granozzi, G. *J. Mol. Struct.* **1988**, *173*, 313–328.
(33) Granozzi, G.; Tondello, E.; Benard, M.; Fragala, I. *J. Organomet. Chem.* **1980**, *194*, 83–89.
(34) Bullock, J. P.; Palazotto, M. C.; Mann, K. R. *Inorg. Chem.* **1991**, *30*, 1284–1293.

Table 2. Acid-Dependent Reactions and Simulation Parameter Values for Fp_2-Catalyzed Reduction of Four Acids

reaction no.	reaction	acid	K	k_f	k_b
6	$Fp^- + HA \rightleftharpoons FpH + A^-$	4-*tert*-butylphenol	0.03	1.0×10^5	3.3×10^6
		4-bromophenol	3.0	1.0×10^5	3.3×10^4
		2-bromophenol	1.00×10^2	1.0×10^5	1.0×10^3
		acetic acid	5.00×10^3	1.0×10^5	2.0×10^1
8	$FpH^{\bullet -} + HA \rightleftharpoons FpH \cdot HA^{\bullet -}$	4-*tert*-butylphenol	1.0×10^3	1.0×10^8	1.0×10^5
		4-bromophenol	1.0×10^4	1.0×10^8	1.0×10^4
9	$FpH^{\bullet -} + HA \rightleftharpoons FpH \cdot HA^{\bullet -}$	4-*tert*-butylphenol	6.3×10^{-5}	1.0×10^4	1.58×10^8
		4-bromophenol	6.9×10^{-4}	1.0×10^4	1.44×10^7
11	$HA + A^- \rightleftharpoons HA_2^-$	4-*tert*-butylphenol	1.58×10^4	1.0×10^8	6.33×10^3
		4-bromophenol	1.58×10^4	1.0×10^8	6.33×10^3
		2-bromophenol	1.58×10^4	1.0×10^8	6.33×10^3
		acetic acid	6.00×10^3	1.0×10^8	1.67×10^4

Table 3. Comparison of Computed Structure of *trans*-Fp_2 to Crystallographic Data[a]

bond/angle	X-ray[b]	DFT[c]
Fe−Fe	2.54	2.51
Fe−C^{cp}	2.13[c]	2.13
C^{cp}−C^{cp}	1.42[c]	1.43
Fe−CO^t	1.76	1.74
Fe−CO^b	1.93	1.92
Fe−C^b−Fe	82.6	81.7
Fe−Fe−C^t	95.7	94.7

[a] Bond lengths are given in Å and angles in deg. [b] Experimental[29] geometric parameters: distances in Å rounded to two decimal places, angles in deg rounded to one decimal place. C^{cp} refers to the carbon atoms of the cyclopentadienyl rings, averaged for the molecule. C^b refers to the bridging COs, and C^t refers to the terminal COs. [c] See the Experimental Section for the source of details on DFT calculations.

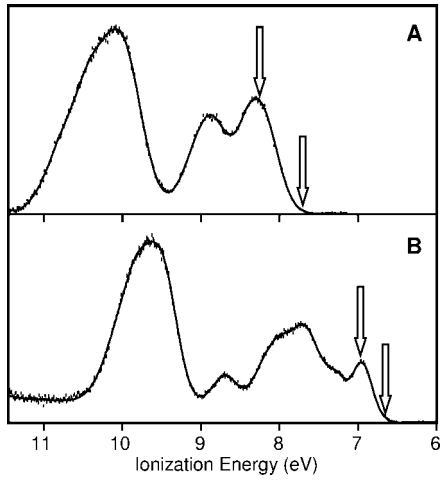

Figure 5. He I gas-phase photoelectron spectra of FpH (A) and Fp_2 (B). The arrows at lower energy mark the adiabatic ionization energies calculated by density functional theory, while those at higher energy correspond to the vertical ionization energies calculated by density functional theory.

simulations are not sensitive to this parameter. Comparisons of calculated and experimental standard potentials and equilibrium constants are summarized in Table 4.

Once FpH is formed, it has been proposed that the complex can react to form the parent dimer, Fp_2, along with H_2. Our calculations, however, indicate that this reaction is slightly uphill by 4.4 kJ/mol. The calculated result is not inconsistent with the experimental results, which indicate negligible reaction during the time scale of the electrolyses.

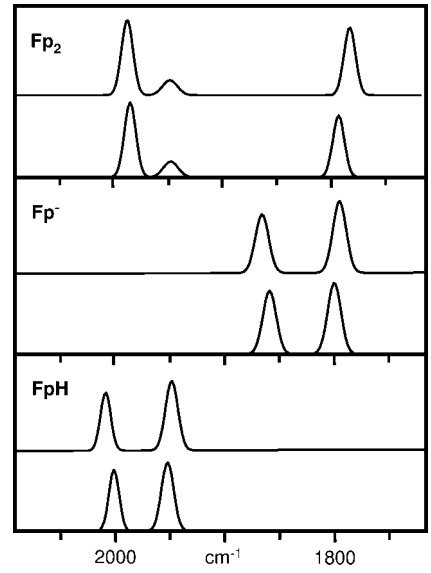

Figure 6. Comparison of the experimental IR spectra in the carbonyl stretching region (top) with the IR absorptions calculated by density functional theory (bottom) for each species. See the Experimental Section for the method of calculation.

According to the calculations, for FpH to be reactive enough to quickly produce dihydrogen, the hydride must first be reduced as in Scheme 1. The calculations result in $E°_7 = -2.50$ V, which agrees very well with the experimental value of −2.55 V. The resulting anion radical, $FpH^{\bullet -}$, then reacts with a proton in solution to form dihydrogen and regenerate the radical monomer, $Fp^{\bullet}$. Using 4-*tert*-butylphenol (HA) as a proton source in the calculations, the formation of H_2, A^-, and $Fp^{\bullet}$ from FpH^- and HA is favored by −33.3 kJ/mol. The resulting radical monomer, $Fp^{\bullet}$, can either be reduced to the anion monomer, Fp^-, or dimerize to the procatalyst, Fp_2, which will be reduced to reform the anion and continue through the catalytic cycle illustrated in Scheme 1. Thus, the computations fully support the mechanism in Scheme 1 and the parameters obtained by either direct measurement or simulation of the electrochemical experiments.

Discussion

The procatalyst, Fp_2, has been shown to be a very effective entry point to the catalysis of hydrogen production from weak

Table 4. Comparison of Calculated, Simulated, and Literature Values of Parameters in the Reaction Scheme[a]

param	value	source
$E°_2$/V	−2.055	this work, calculation
	−2.035	this work, simulation
	−2.1	18d (−76 °C; propionitrile)
	−1.95	18f
K_3/M	59	this work, calculation
	10	this work, simulation[b]
$k_{f,3}$/s^{-1}	fast	this work, simulation[b]
	4.8×10^3	18d (CH_3CH_2CN; extrapolation to 298 K)
	1.2×10^4	18c (extrapolation to 298 K)
	∼500	18f
$E°_4$	−1.01	this work, calculation
	−1.42	this work, simulation[b]
	−1.235	23
$E°^c$	−1.48	This work, calculation
	−1.69	this work, simulation
	−1.84	8e
K_5/M^{-1}	8.0×10^{15}	this work, calculation
$k_{f,5}$/M^{-1} s^{-1}	10^8	this work, simulation[b]
	3.2×10^9	24 (20 °C; cyclohexane)
K_6	2.2	this work, calculation (for HA = 4-*tert*-butylphenol)
	0.03	this work, simulation (for HA = 4-*tert*-butylphenol)
$E°_7$	−2.50	this work, calculation
	−2.59	this work, simulation
pK_a(FpH)	28.3	this work, calculation
	26.0	this work, simulation
	26.7	this work (infrared with 4-*tert*-butylphenol)
	19.4	21
$E°_{Fp^{2+}/Fp_2}$[d]	+0.21	this work, calculation
	+0.22	34
$E°_{FpH^+,FpH}$	+0.72	this work, calculation
	+0.60	this work (irreversible anodic peak potential)

[a] All for acetonitrile solvent at 298 K unless otherwise indicated. "Calculation" refers to DFT calculations in this work. "Simulation" refers to fits of simulations to experimental voltammograms in this work. [b] Simulations insensitive to magnitude of this parameter. [c] For the overall reaction $Fp_2 + 2e^- \rightleftharpoons 2Fp^-$; obtained by combining $E°_2$, K_3, and $E°_4$. [d] Dichloromethane.

acids such as acetic acid. In fact, very substantial catalytic currents are seen with 4-*tert*-butylphenol, which is an acid 5 orders of magnitude weaker than acetic acid. 4-*tert*-Butylphenol is the weakest acid for which reduction catalyzed by metal complexes has been reported. Small but significant catalytic currents are seen with the still weaker acids methanol and water.

Overpotentials for the catalytic reduction range from 0.77 V for 4-*tert*-butylphenol to 1.04 V for acetic acid, significantly larger than those reported for [(μ-1,2-benzenedithiolato)][Fe(CO)$_3$]$_2$ as catalyst (0.4−0.7 V).[16] There is a correlation between catalytic efficiency (as indicated by the catalytic current) and overpotential, with the lowest overpotential being associated with the lowest catalytic current.

There are strong parallels between the behavior seen with Fp_2 and with [(μ-1,2-benzenedithiolato)][Fe(CO)$_3$]$_2$.[16] In both cases the catalyst must be reduced followed by protonation to form a hydride. This hydride cannot react with a weak acid but must be activated by reduction to form an anion with significantly increased hydridicity. Only at that stage does the complex readily transfer hydride to the acid, thus generating dihydrogen.

A key feature in the reaction is the basicity of the anion produced in the initial reduction: Fp^- in the present case. Since protonation to form FpH is the rate-determining step, the most efficient catalysis is seen with acids strong enough to transfer a proton to Fp^-. What is sorely needed in this research is a means of increasing the basicity of the anion without at the same time causing the reduction of the hydride to occur at more negative potentials, thus increasing the overpotential. The results of such efforts will be the subject of future reports.

Experimental Section

Sample Preparation. The Fp dimer [(η^5-C_5H_5)Fe(CO)$_2$]$_2$ was purchased from Aldrich and sublimed for purification immediately prior to use. The FpH for photoelectron data collection was prepared by literature procedures,[35] with the exception of using potassium benzophenone instead of sodium amalgam for the reductant.[36] All compounds were characterized via infrared spectroscopy.

Electrochemistry. Electrochemical instrumentation and the source and treatment of solvents and supporting electrolytes have been reported earlier.[37] All potentials are reported vs the potential of the ferrocenium/ferrocene (Fc^+/Fc) couple measured in the solvent used in the studies: acetonitrile or dichloromethane. The voltammetric experiments were conducted at 298 K. The area of the glassy-carbon working electrode was determined to be 0.0707 cm^2 from cyclic voltammetric studies of the oxidation of ferrocene in acetonitrile using 2.5×10^{-5} cm^2/s as its diffusion coefficient.[38] Studies of Fp_2 with the glassy-carbon electrode led to assignment of a diffusion coefficient of 1.7×10^{-5} cm^2/s. This value in turn was used in studies of Fp_2 with the mercury-film electrode to calibrate the slightly variable area of this electrode. The area ranged from 0.110 to 0.123 cm^2.

Detection of hydrogen after controlled-potential electrolysis was accomplished by gas chromatography, as described earlier.[16]

Photoelectron Data Collection. Photoelectron spectra were recorded using an instrument that features a 36 cm hemispherical analyzer[39] with custom-designed photon source, sample cells, and detection and control electronics, as described previously.[40,41] During He I data collection, the instrument resolution, measured using the full width at half-maximum of the argon $^2P_{3/2}$ ionization, was 0.022−0.029 eV. All of the spectra were corrected for the presence of ionizations caused by other emission lines from the discharge source[42] and for the analyzer transmission (intensity) as a function of electron kinetic energy. In all figures of the data, the vertical length of each data mark represents the experimental variance at that point.[43] FpH sublimed cleanly at room temperature,

(35) Shackleton, T. A.; Baird, M. C. *Organometallics* **1989**, *8*, 2225–2232.
(36) Plotkin, J. S.; Shore, S. G. *Inorg. Chem.* **1981**, *20*, 284–285.
(37) Macías-Ruvalcaba, N. A.; Evans, D. H. *J. Phys. Chem. B* **2006**, *110*, 5155–5160.
(38) Hong, S. H.; Kraiya, C.; Lehmann, M. W.; Evans, D. H. *Anal. Chem.* **2000**, *72*, 454–458.
(39) Siegbahn, K.; Nordling, C.; Fahlman, A.; Nordberg, R.; Hamrin, K.; Hedman, J.; Johansson, G.; Bergmark, T.; Karlsson, S. E.; Lindgren, I.; Lindberg, B. *ESCA: Atomic, Molecular, and Solid State Structure Studied by Means of Electron Spectroscopy*; Almqvist & Wiksells: Uppsala, Sweden, 1967.
(40) Lichtenberger, D. L.; Kellogg, G. E.; Kristofzski, J. G.; Page, D.; Turner, S.; Klinger, G.; Lorenzen, J. *Rev. Sci. Instrum.* **1986**, *57*, 2366.
(41) Rajapakshe, S. A.; Gruhn, N. E. ; Paz-Sandoval. M. A.; Fuentes, A. G.; Navarro-Clemente, M. E.; Lichtenberger, D. L. Abstracts of Papers, 229th National Meeting of the American Chemical Society;March 13−17, 2005, San Diego, CA; American Chemical Society: Washington, DC, 2005;INOR-637.
(42) Turber, D. W.; Baker, C.; Baker, A. D. ; Brundle, C. R. *Molecular Photoelectron Spectroscopy: A Handbook of He 584 Alpha Spectra*; Interscience: New York, 1970.
(43) Lichtenberger, D. L.; Copenhaver, A. S. *J. Electron Spectrosc. Relat. Phenom.* **1990**, *50*, 335–352.

with no visible changes in the spectra during data collection. Fp dimer sublimed cleanly between 95 and 120 °C.

Computations. All computations were performed using ADF2006.01d.[44] Computational methods have been described previously.[16] For comparison of the calculated gas-phase CO stretching frequencies to the experimental solution-phase IR spectra, the calculated frequencies were scaled by a factor of 0.993 or roughly 14 cm^{-1}. Each computed IR absorption peak was broadened with a Gaussian function, as in previous work.[45] The absorption peaks were broadened by 7 cm^{-1} to visually compare to the experimental peaks.

Acknowledgment. The support of the National Science Foundation through the Collaborative Research in Chemistry program, Grant No. CHE 0527003, and Grant Nos. CHE 0416004 (D.L.L.) and CHE 0715375 (D.H.E.) are gratefully acknowledged.

Supporting Information Available: Text and figures giving simulations of catalyzed reduction of 4-*tert*-butylphenol by Fp_2 for additional scan rates and acid concentrations and one other Fp_2 concentration and a discussion of the reactions used in the mechanism, examples of the fits of simulation to background-corrected voltammograms of Fp_2 in the presence of four different acids with scans including only the first reduction and the oxidation peak, examples of simulations of Fp_2 reduction in the presence of 4-bromophenol for wide scans that include the catalytic peak, and the infrared spectrum in the carbonyl stretching region of a 1:1 mixture of Fp^- and 4-*tert*-butylphenol. This material is available free of charge via the Internet at http://pubs.acs.org.

OM800366H

(44) ADF200601d; SCM, Theoretical Chemistry, Vrije Universiteit, Amsterdam, 2006; http://www.scm.com.

(45) Borg, S. J.; Tye, J. W.; Hall, M. B.; Best, S. P. *Inorg. Chem.* **2007**, *46*, 384–394.